CAUSE OF SECONDARY HARDENING IN Cr–Mo–V WELD METAL DURING LONG-TERM HEAT EXPOSURE

P. MOHYLA, I. HLAVATY and **P. TOMCIK**
Technical University of Ostrava, Czech Republic

Results of microstructural analysis quantified changes in the dispersion phase in Cr–Mo–V weld metal during exposure in the sub-creep range are presented. The hypothesis that changes in the dispersion of MX particles during long-term heat exposure are significant has been confirmed by presented results.

Keywords: *CrMoV steel welds, sub-creep range, secondary hardening, vanadium carbides and carbonitrides, microstructural analysis, image analysis*

Low-alloy creep-resistant steels of 0.5 % Cr–0.5 % Mo–0.3 % V type are used in power industry for fabrication pipes and tubes. Their long-term creep resistance, expressed as creep rupture strength (CRS) after 105 h, is significantly higher in comparison with 2.25 % Cr–1 % Mo steels. The other significant property of creep-resistant steels containing vanadium is their demanding technological processing, which stems from the dominant affect of the dispersion phase on their mechanical properties. Parameters of dispersion phase are very sensitive on heat treatment. Vanadium carbides and carbonitrides (MX particles), which precipitate mainly during tempering, play the key role in Cr–Mo–V steels.

However, during long-term heat exposure the number, mean size and mean spacing of particles are changed. These changes significant influence mechanical properties and thereby even the durability and operating reliability of power equipment. Operation of the tested steel 14MoV6-3 in the sub-creep temperature range (maximum 480 °C) causes secondary hardening, accompanied by a decrease of impact toughness. The mentioned secondary hardening is especially pronounced in welded joints tempered at temperatures lower than those required by the material specification, i.e. temperatures lower than 720 °C.

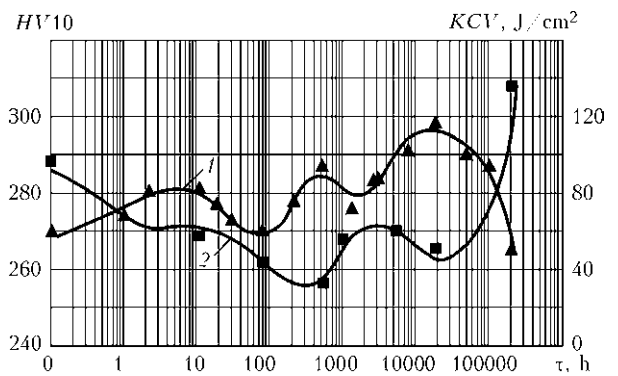

Figure 1. Hardness (*1*) and impact toughness (*2*) of weld metal at operating temperature of 450 °C (tempering at 680 °C for 2 h)

Figure 1 shows the changes in hardness and impact toughness of weld metal tempered at 680 °C. Mechanical properties were measured according to relevant standards [1]. Microanalysis using an electron microscope was performed to confirm additional precipitation of MX particles in weld metal of 14MoV6-3 steel.

Electron microstructural analysis. Weld metal samples tempered to 680 °C and after subsequent heat exposure served as material to be studied. Parameters of simulated heat exposure were as follows: for sample 1.0 — initial condition; for sample 1.11 — after annealing at 500 °C for 23.4 h; for sample 1.1 — after annealing at 550 °C for 50.4 h; and for sample 1.20 — after annealing at 550 °C for 546.5 h

These samples are highlighted in Figure 2. Parameters of simulated heat exposure are recalculated to operating temperature of 450 °C.

Structure-phase analysis of weld metal. The weld metal microstructure contains a mixture of ferrite and bainite. The electron-microscope study was conducted using transmission electron microscope (TEM) of JEM 200CX type, equipped with an energy dispersion analyser. Identification of minority phases was performed using a combination of electron diffraction and qualitative energy dispersion analysis of particles on extraction carbon replicas. Thin metal foils were prepared by jet polishing in the electrolyte (95 % CH_3COOH and 5 % $HClO_4$) at room temperature and voltage U = 80 V.

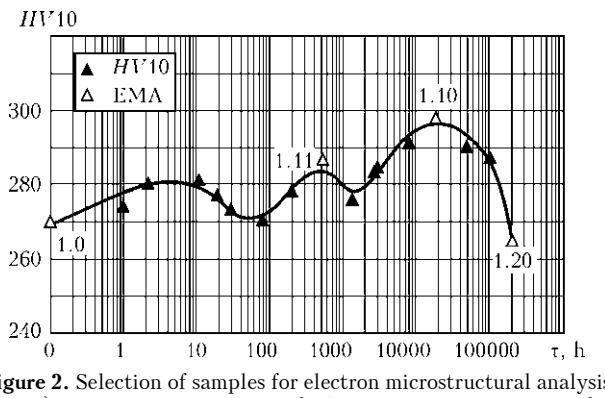

Figure 2. Selection of samples for electron microstructural analysis (EMA), operating temperature of 450 °C, tempering at 680 °C for 2 h

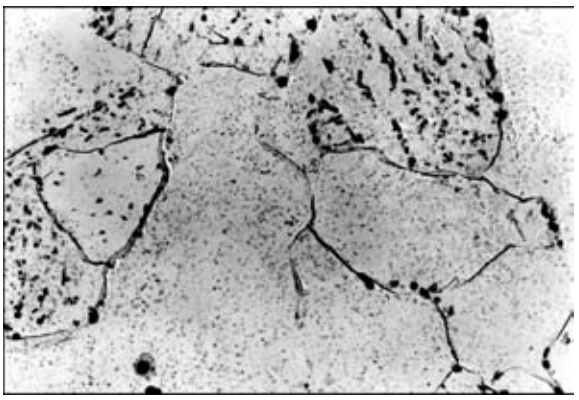

Figure 3. Distribution of precipitate on extraction carbon replica for sample 1.0 (×9000)

Results of minority phase study in the samples were as follows: MX, M_3C in sample 1.0; MX, M_3C in sample 1.11; MX, M_3C in sample 1.1; and MX, M_3C in sample 1.20. It is evident that all samples contained particles of cementite and MX, where M = = V, and X = C and N. A typical example of precipitate distribution in extraction carbon replicas is presented in Figure 3. Fine MX particles precipitated inside ferrite and bainite-ferrite grains, while the relatively coarse cementite grains usually lined the bainite-ferrite boundary. The fibrous morphology of MX particles observed in works [2, 3] was not seen in studied samples. Furthermore, weld metal included numerous globular particles of complex silicon, manganese and titanium oxides.

Dislocation density was determined in bainite-ferrite plates. Dislocation density was calculated using the Ham's method:

$$\rho = \left(\left(\frac{N_1}{L_1}\right) + \left(\frac{N_2}{L_2}\right)\frac{1}{t}X\right) \ (\text{m}^{-2}), \qquad (1)$$

where N_1, N_2 is the number of intersections of two parallel lines with dislocations; L_1, L_2 is the total length of lines; $t = 125$ nm is the foil thickness selected; X is the factor considering the share of non-visible dislocations for the selected imaging diffraction conditions.

The density of dislocations in individual samples was assessed on photographs with a total magnification of 109,000 (Figure 4). Measurement results (arithmetic mean and standard deviation) were as follows, $\rho \cdot 10^{-14}$ m^{-2}: in sample 1.0 — 4.91 ± 0.94; in sample 1.11 — 4.26 ± 0.97; in sample 1.1 — 4.50 ± ± 0.66; and in sample 1.20 — 3.60 ± 0.95. It is evident that the differences in dislocation density in bainite-ferrite are insignificant in measured samples.

Image analysis. Image analysis methods enable determination of important parameters characterising the dispersion phase, such as mean particle size or number of particles per unit area, and subsequently the calculation of the number of particles per unit volume or mean inter-particle spacing. Our objective was the determination of these parameters for MX particles in the case of individual samples, i.e. during different stages of long-term heat exposure of weld metal in the sub-creep region. Three samples were selected for these purposes, namely 1.0, 1.1 and 1.20 (see Figure 2). Extraction carbon replicas were made from these samples and photographed subsequently with a magnification of 151,000. The photograph of sample 1.20 is presented in Figure 5. All the photos were converted into electronic images. These images were subject to image analysis using Micro Image 4 software. The result is a set of output values, namely particle area A_x, maximum diameter D_{max}, mean diameter D_{mean}, minimum diameter D_{min}, equivalent particle diameter D_{eq} and the particle area — total photograph area ratio P_A, as well as the number of particles n_0, number of photographs, and total monitored area A_0.

The image analysis for each sample was performed on several photos, therefore the total monitored area A_0 is the sum of the individual photograph areas.

The number of particles per unit area n_s was calculated as a proportion of the number of monitored particles n_0 and monitored area A_0:

$$n_s = \frac{n_0}{A_0}. \qquad (2)$$

Calculation of the number of particles per unit volume was performed using a formula from the Ashby and Ebeling paper [4], which deals with the determi-

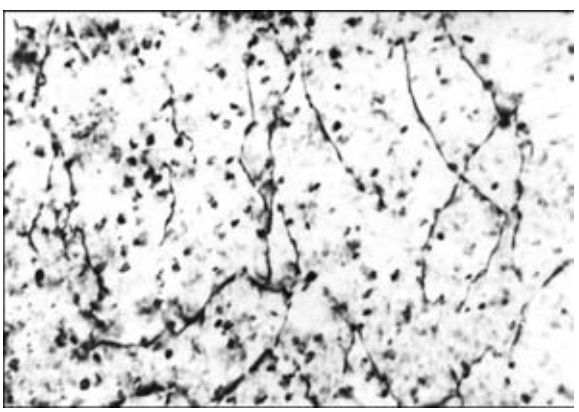

Figure 4. Dislocation substructure (×109,000) of weld metal (thin foil, sample 1.20)

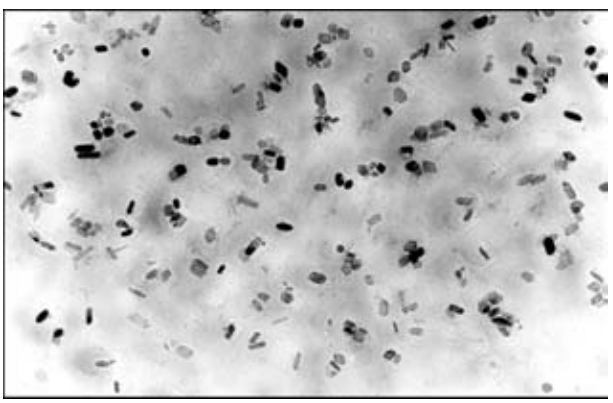

Figure 5. Dispersion of MX particles (×151,000) in the weld metal microstructure (bainite, extraction carbon replica, sample 1.20)

Calculation results for n_s, n_v and λ

Sample No.	A_x, nm^2	d_{eq}, nm	$n_s \cdot 10^{-14}$, m^{-2}	$n_v \cdot 10^{-22}$, m^{-3}	λ, nm, acc. [7]	λ, nm, acc. [8]
1.0	168.24 ± 10.59	13.65 ± 0.33	2.13037	1.79595	52.72	32.92
1.1	124.01 ± 3.24	12.10 ± 0.15	7.96117	7.08676	24.26	13.68
1.20	246.10 ± 8.04	16.91 ± 0.29	2.81644	1.82597	43.10	25.46

nation of number, size and spacing of secondary phase particles in extraction replicas:

$$\frac{n_v}{n_s} = \frac{1}{d_{eq}} \left\{ 1 + \left(\frac{\sigma}{d_{eq}} \right)^2 \right\}, \quad (3)$$

where n_v is the number of particles per unit volume; n_s is the number of particles per unit area; d_{eq} is the equivalent spherical particle diameter (arithmetic mean); α is the standard deviation of equivalent diameter

The equivalent particle diameter d_{eq} is the diameter of the projection of an equivalent spherical particle (circle) into a section plane of the same area as is the area of the real particle (general shape). The d_{eq} value was determined from a measured particle area A_x according to the following formula:

$$d_{eq} = \sqrt{\frac{4A_x}{\pi}}. \quad (4)$$

Particle spacing was determined according to the plane square particle arrangement model, which is suitable for assessing dispersion hardening of low-alloy steel [5]. The calculation was performed in two alternatives as per paper [6]. According to Kelly and Nicolson [7] the mean distance of particle edges is determined from

$$\lambda = (n_v d_{eq})^{-1/2} - \sqrt{\frac{2}{3}}\, d_{eq}. \quad (5)$$

According to Ashby [8], equation (5) is rectified, due to mutual interaction of dislocation sections after overcoming a particle, as follows:

$$\lambda = 0.69(h_v d_{eq})^{-1/2} - \sqrt{\frac{2}{3}}\, d_{eq}, \quad (6)$$

where d_{eq} is the equivalent particle diameter; λ is the mean particle spacing; n_v is the number of particles per unit volume

Calculation results are summarised in the Table.

So, dominant observed processes are the additional precipitation and coarsening of MX particles. Sample 1.1 with the highest hardness during heat exposure (see Figure 2) represents an area of additional precipitation of MX particles. This is indicated by the highest number of particles per unit volume, smallest size and smallest mean inter-particle spacing in comparer to the other samples. In comparison with the initial condition (sample 1.0), the number of particles increased almost 4 times and the mean inter-particle spacing dropped more than 2 times. In comparison, sample 1.20 represents an area of coarsening of secondary particles. This is confirmed by the largest mean particle area, significant decrease in number of particles (approximately by 4) and almost a doubled increase in mean inter-particle spacing compared to sample 1.1. The significant influence of the secondary phases on mechanical properties of 14MoV6-3 steel is also confirmed by the fact that the dislocation density remained almost unchanged during observed heat exposure.

CONCLUSION

The dispersion of MX particles of 0.5 % Cr–0.5 % Mo–0.3 % V steels changes its parameters during steel tempering and subsequent long-term heat exposure. These changes significantly influence the material mechanical properties. Operation of 0.5 % Cr–0.5 % Mo–0.3 % V weld metals in the sub-creep range causes secondary hardening accompanied by a degradation of plastic properties. This hardening is pronounced especially in welded joints tempered at lower tempering temperatures (of about 680 °C). Proper post-weld heat treatment at temperature of about 720 °C can be recommended for 14MoV6-3 steel.

Acknowledgements. *This result of project LN00B029 was supported by the Ministry of Education of Czech Republic.*

1. Krejci, L. (2006) Mechanical testing of welded joints. In: *Proc. of Seminar «Svarovaci den 2006»*. Ostrava: TU, 40–47.
2. Schmidova, E., Svanda, P., Vesely, D. et al. (2009). Mechanism of degradation of stabilised corrosion-resistant steel during the welding cycle. *Anti-Corrosion Methods and Materials*, 56(**4**), 206–217.
3. Bosela, M., Vinas, J., Varga, V. (2001) The analysis of welds-on with resistance against of high area pressure. In: *Proc. of 9th Int. Sci. Conf.* (Trnava, 25–26.10.2001). Bratislava: STU, 186–191.
4. Ashby, M.F., Ebeling, R. (1966) On the determination of the number, size, spacing and volume fraction of spherical second-phase particles from extraction replicas. *Transact. of Metallurgical Society of AIME*, **236**.
5. Prnka, T. (1975) *Diss. for Technical University of Ostrava.*
6. Purmensky, J. (1978) *Diss. for Technical University of Ostrava.*
7. Kelly, A., Nicholson, R.B. (1963) Precipitation hardening. *Progress in Material Sci.*, **10**.
8. Ashby, M.F. (1969) *Physics of strength and plasticity*. MIT Press, 113.